Chemosphere 376 (2025) 144255

Contents lists available at ScienceDirect

Chemosphere

journal homepage: www.elsevier.com/locate/chemosphere

Concerns linked to highly dispersed iron anchored within graphitic carbon nitride, is it a truly promising material to drive heterogeneous photo-Fenton treatments?

Simone Pellegrino, Iván Sciscenko [*,1], Fabrizio Caldera , Claudio Minero, Enzo Laurenti, Marco Minella

University of Turin, Department of Chemistry, Via Pietro Giuria 7, 10125, Turin, Italy

HIGHLIGHTS

- The stability of carbon nitride is usually overlooked.
- Fe-g-C_3N_4/H_2O_2 releases more nitrates than g-C_3N_4/H_2O_2.
- Fe-g-C_3N_4 is less stable than g-C_3N_4 due to the involved reactions.
- Formed reactive species oxidise g-C_3N_4 structure rather than the pollutants.

GRAPHICAL ABSTRACT

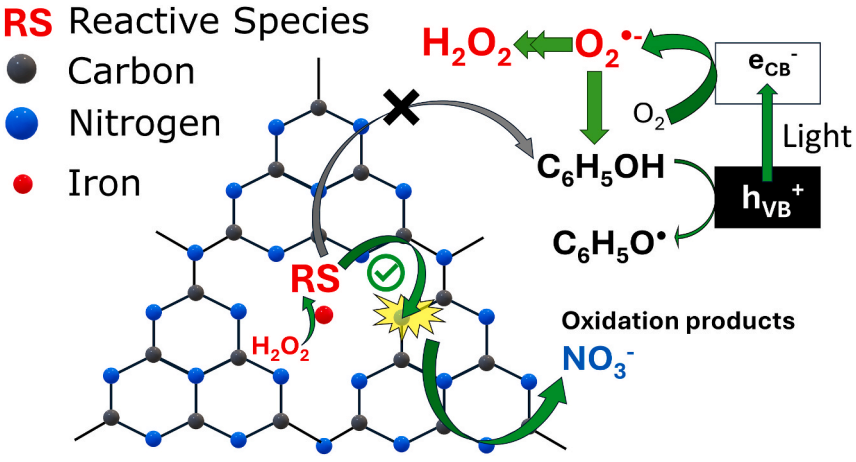

ARTICLE INFO

Handling editor: Xiangru Zhang

Keywords:
Contaminants of emerging concern
Carbon nitride stability
Heterogeneous photocatalysis
Water treatment

ABSTRACT

The precipitation of iron at pH > 4 is one of the main drawbacks of any Fenton-based process. Among the engineered solutions, the incorporation of iron within the wide cavities of graphitic carbon nitride (g-CN) has recently gained momentum. However, most works employing Fe-g-CN materials usually employ high H_2O_2 concentrations (>25 mM) to observe considerable pollutant abatements (without or with UV–vis light irradiation, i.e., by heterogeneous dark- or photo-Fenton processes, respectively). To gain further insights into this issue, in this work, Fe-g-CN, with different amounts of iron, were synthesised by thermal polycondensation of melamine and $FeCl_3 \cdot 6H_2O$ as precursors and compared its performance with the g-CN alone. Under UV-A light, a content of 0.2% w/w of iron in the g-CN was optimal to improve the oxidative performances of target pollutants (phenol and sulfamethoxazole 100 μM, respectively), higher Fe-loadings decreased the photocatalytic performances with respect to g-CN. Interestingly, this trend was inversed when adding H_2O_2 1 mM, being the pollutant

* Corresponding author.
E-mail address: ivanmatias.sciscenko@unito.it (I. Sciscenko).
[1] Previous institution: Universitat Politècnica de València, Departamento de Ingeniería Textil y Papelera, Plaza Ferrándiz y Carbonell s/n, 03801 Alcoy, Spain.

https://doi.org/10.1016/j.chemosphere.2025.144255
Received 19 December 2024; Received in revised form 21 February 2025; Accepted 22 February 2025
Available online 4 March 2025

removal by g-CN faster than that by Fe-g-CN (for phenol, $k_{obs} = 8.02 \times 10^{-2}$ min^{-1} and 2.83×10^{-2} min^{-1}, respectively), opposed to expectations. Furthermore, $HO^{\bullet}$, $HO_2^{\bullet}$ or $^1O_2$ were barely detected by Electron Paramagnetic Resonance, indicating that the reactive species should oxidise the g-CN rather than react with the spin traps. Finally, although g-CN oxidation was not observed by typical characterisation techniques (such as FT-IR/ATR), we have observed 6 times more nitrates formation by illuminated Fe-g-CN than g-CN, indicating that iron enhances the self-oxidation of illuminated carbon nitrides. Our results demonstrate that iron incorporation in g-CN might be not as convenient as usually stated in the literature, as the stability of the photocatalyst is drastically reduced, releasing nitrates and possibly decreasing the material's lifetime.

Abbreviations

TEMP	2,6,6-tetramethylpiperidine
DMPO	5,5-dimethylpyrrolidine-N-oxide
AOPs	advanced oxidation processes
ATR	attenuated total reflectance
e^-_{CB}	conduction band's electrons
EPR	electron paramagnetic resonance
FFA	furfuryl alcohol
g-CN	graphitic carbon nitride
IPA	isopropyl alcohol
p-BQ	*p*-benzoquinone
ROS	reactive oxygen species
RS	reactive species
IC	total inorganic carbon
TOC	total organic carbon
h^+_{VB}	valence band's holes
XRD	X-ray diffraction

1. Introduction

Reclaimed water (treated wastewater for reuse) is known for its potential to enhance agricultural output as well as foster rural development (alongside supporting a circular economy perspective). Its use for crop irrigation has been historically led by countries with semi-arid regions and where agriculture is among its more important economic activities, such as, United States, Spain, Israel or Australia. To accomplish stipulated quality standards, wastewater treatment plants are required to couple a tertiary, or even quaternary, steps at their facilities. In this sense, advanced oxidation processes (AOPs) are among the most efficient treatments towards the abatement of emerging contaminants and resistant genes/bacteria (Christou et al., 2024).

The Fenton reaction is a well-known AOP where the reactive species (e.g., $HO^{\bullet}$ or FeO^{2+}) used to eliminate pollutants and microorganisms are generated during the H_2O_2 decomposition catalysed by iron ions. Under UV–visible irradiation (photo-Fenton), due to the ligand-to-metal charge transfer transition of $Fe(OH)^{2+}$ and $Fe(HO_2)^{2+}$, the efficiency of this treatment increases as a consequence of the acceleration in the Fe (III) reduction (that is usually the rate-limiting step), resulting in a more significant generation of reactive species and faster pollutant degradation rates (Miklos et al., 2018; Sciscenko et al., 2024b). Furthermore, to obtain considerable pollutant degradation rates at neutral pH values, iron chelating agents are required to avoid the formation of insoluble ferric (oxy)hydroxides at pH > 4 (Bertolotti et al., 2022; Sciscenko et al., 2021). However, since adding an external reagent increment costs and quenches reactive species, the incorporation of Fe(II, III) within the wide cavities of graphitic carbon nitride (g-CN) has been gaining noticeable interest in the last years as a way to drive photo-Fenton reactions at neutral pH as well as having the intrinsic advantage of reutilization after use (Fei et al., 2021; Mao et al., 2022; Wang et al., 2020; Yong et al., 2024).

g-CN is a polymer constituted by heptazine units with molecular formula of $C_6N_9H_3$ (Liebig's melon), whose stoichiometry is, however, usually denoted as C_3N_4 by convention (Lau et al., 2015; Minella et al., 2021). Although known since 1835, the utilisation of this metal-free semiconductor as a potential photocatalyst to accelerate different reactions (e.g., H_2O_2 green production (Haider et al., 2019; Sciscenko et al., 2024a)) has attracted global interest only in the last fifteen years (Ben-Refael et al., 2020). Due to its electronic properties, g-CN is most likely applicable towards reductive reactions rather than oxidative ones. For this reason, its combination with iron has been proposed as a valuable material to drive *in situ* heterogeneous photo-Fenton reactions due to the potential formation of H_2O_2 from the reduction of dissolved oxygen as well as the acceleration of the iron cycle by photogenerated conduction band electrons (e^-_{cb}), respectively, avoiding the logistic problems related to H_2O_2 management and iron sludge formation (Chen et al., 2023; Coha et al., 2021; Lin et al., 2022).

When critically analysing the works employing dark or illuminated Fe-g-CN systems, far from an *in situ* photo-Fenton, it can be observed that an external addition of high H_2O_2 concentrations (>50 mM = 1,700 mg L^{-1}) is required to observe fast pollutants degradation rates (An et al., 2018; Ding et al., 2022; Li et al., 2021; Luo et al., 2020; Wang and Nan, 2020). The use of high concentrations of peroxides could certainly discourage the use of this type of photocatalysts. Moreover, the reasons for applying these unpractical high H_2O_2 concentrations are usually overlooked, which could be related to the fact that produced reactive species should react with the g-CN structure rather than with the target pollutants. As a matter of fact, the work by Xiao et al. (2017) was the first -and still one of the few- to report that high production of $HO^{\bullet}$ (generated when combining g-CN with ozonation under simulated sunlight irradiation) degrades the g-CN, leading to cyameluric acid as the main oxidation by-product, and CO_2, H_2O and NO_3^- as mineralization products (Xiao et al., 2017). In the same line, similar works recently reported the efficiency decay towards pollutant degradation by illuminated g-CN due to its self-oxidation by generated reactive oxygen species (ROS) (Wang et al., 2021) or even chloride radicals (Li et al., 2023).

In this work, a holistic study was carried out on Fe-g-CN materials with different iron content, with particular focus on the reactive species involved in the degradation mechanisms of model contaminants. While others have reported the use of Fe-g-CN as a promising photocatalyst to perform photo-Fenton at circumneutral pH values, this work highlights the critical need for stability controls and to bear in mind that ROS, and/or high valent iron species, might degrade with higher probability the g-CN structure than the target pollutants, which could eventually cause plausible repercussions on its application in wastewater treatment plants.

2. Experimental

2.1. Reagents and material

Phenol, sulfamethoxazole, *p*-benzoquinone, methanesulfonic acid, 4-aminoantipyrine, glacial acetic acid, horseradish peroxidase, H_2O_2 33%, H_3PO_4 85%, HNO_3 65%, HCl 37%, methanol HPLC grade and isopropyl alcohol (IPA) were purchased from VWR. Melamine, furfuryl alcohol, humic acids and $HClO_4$ 70%, were obtained from Sigma Aldrich. K_2CO_3, Na_2SO_4, NaCl, NaOH, $NaNO_3$, $NaHCO_3$, $NaH_2PO_4{\cdot}H_2O$,

$Na_2HPO_4{\cdot}12H_2O$ and *o*-phenanthroline were acquired from Alfa Aesar. $FeCl_3{\cdot}6H_2O$, dimethyl sulfoxide (DMSO) and sodium acetate were bought from Panreac. Ultra-pure water was obtained through Merck-Millipore EQ(7000) water system (TOC <2 ppb, resistivity ≥18.2 mΩ cm).

Phenol and sulfamethoxazole standard solutions were stored in the fridge at 4 °C until use, which were stable against hydrolysis degradation for several months.

2.2. Photocatalysts synthesis

Fe(III) incorporation into melon structure (Fe-g-CN) was carried out by a procedure based on other works (Fei et al., 2021; Wang et al., 2020). Basically, 2 g of a mixture containing different proportions of $FeCl_3{\cdot}6H_2O$ and melamine were placed into alumina crucibles and placed inside a horizontal tubular oven (Lenton LHC 12/750); the iron-melamine mixture was carried out by grinding both reagents with a ceramic mortar for, approximately, 30 s; different grinding times, mixing methods, and mortar materials were considered and studied in section 3.1.1. Afterwards, the Fe(III)-melamine mixture was subjected to a thermal polycondensation reaction under anoxic conditions (N_2 atmosphere) at 500 °C for 2 h (employed ramp rate, 5 °C min^{-1}). The obtained materials were grounded with a ceramic mortar until obtaining a powder and subsequently washed with ultra-pure water and absolute ethanol to remove non-incorporated iron and low molecular weight carbon nitrides reaction intermediates, respectively. The obtained Fe-g-CN were named according to the percentage of Fe(III) within the initial mixture with melamine (e.g., Fe-g–CN–(0.07) means that 100 g of melamine-$FeCl_3{\cdot}6H_2O$ mixture contained 0.07 g of Fe(III), i.e. 0.07% w/w).

The direct photodegradation by UVA light and the adsorption on the developed photocatalysts of each pollutant (employing 100 μM as initial concentration) was negligible (<10%) for at least 3 h of the experiment.

2.3. Pollutant degradation experiments

The dark-Fenton and photo-Fenton activity of the synthesised materials were evaluated by measuring the degradation kinetics of 100 μM phenol or sulfamethoxazole (model pollutants). g-CN (or Fe-g–CN–(0)) was used as reference material to assess the effect of iron in the overall oxidative process. In all cases, aqueous suspensions of 1.65 g L^{-1} (value selected based on previous work (Sciscenko et al., 2024a)) of Fe-g–CN–(%Fe) were employed, and the initial pH was adjusted to 7.0 ± 0.2 with NaOH 0.1 M (Metrohm 691 pH Meter). Previous addition of H_2O_2 and/or irradiation (employing UVA light, Philips BLB fluorescent lamp, λ_{max} = 365 nm), the photocatalyst suspension was previously sonicated (Branson 2800 sonicator) for 1 h to exfoliate the material. 5 mL of sonicated suspension were afterwards transferred into closed cylindrical Pyrex cells (total volume 33 mL, cut-off at 295 nm) and continuously mixed by magnetic stirring. Sampling was performed at different time intervals and the material was removed by filtering with VWR syringe filters (PTFE, 0.45 μm pore diameter). Reactions were stopped by the addition of methanol in excess to quench the plausible dark-Fenton process. Periodic checks were carried out to verify the irradiance constancy (20 W m^{-2}) using CO.FO.ME.GRA multimeter with 295–400 nm probe.

The H_2O_2 addition effect (besides the one photogenerated by the synthesised materials in illuminated experiments) was studied in the range of 1–25 mM, whereas the water constituents' effect was studied by adding 0.1–10 mM of NO_3^-, $H_2PO_4^-/HPO_4^{2-}$, HCO_3^-, Cl^- and SO_4^{2-} (main anions present in natural waters), or 0.1–100 mg L^{-1} of humic acids at synthetic aqueous matrices with phenol spiked.

Finally, the efficiency of the Fe-g–CN–(%Fe) was studied on real water matrices: i) tap water, ii) aquaculture water, and iii) primary effluent wastewater. Results from characterisations of the aforementioned water matrices are shown in Table S1.

2.4. Analytical measurements

Total iron concentration was measured by spectrophotometric method (Cary 100 Scan UV–Visible spectrophotometer) based on the formation of Fe(II)-*o*-phenanthroline complex quantified at λ = 510 nm (ISO 6332:1988). The same instrument was used for H_2O_2 concentration (formed or residual when added externally) determination, based on the methodology described in Zhou et al. (2006) work.

Target contaminants concentration was determined by UV–visible high-performance liquid chromatography (HPLC, YL 9300, C18 column Lichrospher R100, C18, 5 μm) coupled to UV/vis detector employing as mobile phase H_3PO_4 5 mM: CH_3OH, 75:25 (% v/v) 1 mL min^{-1} elution flow, and 35 °C column temperature. Phenol was measured at λ = 220 nm and sulfamethoxazole at 265 nm (retention time 7.3 and 9.4 min, respectively).

Ions concentrations were measured with a Dionex DX 500 Ion Chromatograph equipped with a ED-40 conductometric detector. For anions, a Dionex IonPac AS9-HC column (4 × 250 mm) and Thermo-Scientific ADRS 600 4 mm conductivity suppression unit were used, whereas for cations, a Dionex IonPac CG12A column (4 × 250 mm) and Thermo-Scientific CDRS 600 4 mm conductivity suppression unit were employed. The chromatographic runs were performed in isocratic mode (flow = 1 mL min^{-1}), employing K_2CO_3 9 mM or methanesulfonic acid 20 mM as mobile phases for the anionic and cationic determination, respectively.

Total organic carbon (TOC) and inorganic carbon (IC) were measured with a Shimadzu TOC-V CSH equipment with ASI-V autosampler, respectively.

2.5. Reactive oxygen species scavenging and detection

200 μM of selective quenching agents were firstly employed to tentatively observe the predominant role of specific reactive species, namely: isopropanol for hydroxyl radical (IPA, k ($HO^\bullet$) = 1.9×10^9 M^{-1} s^{-1}), furfuryl alcohol for singlet oxygen (FFA, k ($^1O_2$) = 1.2×10^8 M^{-1} s^{-1}), dimethyl sulfoxide for high valent iron species (DMSO, k (Fe(IV) = 1.3×10^5 M^{-1} s^{-1}) and *p*-benzoquinone for superoxide (p-BQ, k ($O_2^{\bullet-}$) = 9.0×10^8 M^{-1} s^{-1}) (Appiani et al., 2017; Buxton et al., 1988; Cai et al., 2024; Pestovsky and Bakac, 2006). ROS formation was later confirmed by electron paramagnetic resonance (EPR, X-band Bruker EMX spectrometer), employing 17 mM of spin traps, 5,5-dimethylpyrrolidine-N--oxide (DMPO, detection of $HO^\bullet$ and $HO_2^\bullet$) and 2,6, 6-tetramethylpiperidine (TEMP, detection of $^1O_2$).

2.6. Characterisations

The stability of the incorporated iron within the g-CN structure was determined by measuring the total dissolved iron (by spectrophotometry, see section 2.4) when suspended in an acidic solution of HCl 0.01 M, as well as after the photocatalytic phenol degradations.

The iron content of the synthesised materials was measured by a first thermal decomposition treatment, calcinating the desired Fe-g–CN–(X %) at 900 °C (g-CN is stable until 700 °C (Zhu et al., 2014)), for 1 h (muffle furnace ZA model, T_{max} 1100 °C), and the remaining ashes were weighted and dissolved in 10 mL of $HNO_{3(c)}$:$HCl_{(c)}$ (molar ratio 1:3); the total iron was measured from the latter acidic digestion. The photocatalysts' optical properties were assessed by diffuse reflectance (Varian Cary 5000 UV–Vis–NIR). The chemical and crystallinity information were studied with Fourier-Transform Infrared Spectroscopy/Attenuated Total Reflectance (FT-IR/ATR, iD7-ATR Thermo Scinetific, equipped with Nicolet iS5 spectrophotometer) and X-ray diffraction (XRD, Panalytical Empyrean diffractometer, equipped with a CuKα radiation and a PIXCel3D detector), respectively. The C, N, and H content were measured by elemental analysis (Thermo Fisher CHNS-O analyser, Flash EA 1112 series) as performed in previous work (Sciscenko et al., 2024a). When needed, the materials were also characterised after irradiation.

3. Results and discussion

3.1. Preliminary experiments

3.1.1. Iron – melamine mixing

It is usually stated that the mixing between iron and the g-CN precursor might affect the photocatalytic properties of the obtained materials (An et al., 2018; Ding et al., 2022; Wang and Nan, 2020). To confirm if this procedure is worth the effort (as well as knowing the best way of preparing the material), we have compared the phenol photocatalytic degradations by UVA/Fe-g–CN–(0.28) by changing the mixing method. We have compared: i) different mixing times with the same mortar (grinding for 30 s vs. 5 min), ii) comparing (with the same mixing time) the one obtained with the ceramic mortar against agate mortar and the one reached with gross mixing (placing both reagents inside a closed flask and performing a vague agitation), and iii) adding the melamine into a concentrated solution of Fe(III), and afterwards placing the suspension inside an oven at 40 °C until water evaporation. As shown in Fig. 1A, no significative difference in the phenol degradation rates were observed with the Fe-g–CN–(0.28) obtained through different iron-melamine mixing techniques (85% phenol removal in 3 h), except for the one prepared with the vague agitation of both reagents, resulting in slightly slower phenol degradation kinetics. These results suggest that $FeCl_3$ is firstly dissolved in the liquid melamine (melting point, 345 °C) before the cyclisation reaction starts (Lotsch and Schnick, 2005), therefore, the initial mixing technique is not as relevant as usually stated. This is an important observation, as a simple mixing method is detrimental towards a plausible scale-up of the synthesis.

3.1.2. Detection of optimal iron content

Different iron contents were analysed for improving the phenol degradation rates under UVA irradiation compared to melon (Fe-g–CN–(0), or simply g-CN from now on); the technique of grinding in ceramic mortar for a 30 s was employed in each case.

As shown in Fig. 1B, an iron content of 0.07% (in the melamine-$FeCl_3{\cdot}6H_2O$ mixture) was enough to improve by a factor of 1.5 times the phenol oxidation rate with respect to g-CN ($k_{obs} = 2.3 \times 10^{-2}$ min^{-1} and 1.5×10^{-2} min^{-1}, respectively). Noteworthy, when adding higher iron amounts, the phenol oxidation rate exhibited a marked decrease: Fe-g–CN–(0.16) led to a $k_{obs} = 1.3 \times 10^{-2}$ min^{-1}, whereas with Fe-g–CN–(0.28) it was of 9.1×10^{-3} min^{-1}. This is in line with what was suggested in other works, where additions of excessive iron amounts promote the aggregation of the latter, interfering with the thermal polycondensation of g-CN, and eventually reducing the photocatalytic activity of Fe-g-CN (An et al., 2018; Lei et al., 2020).

As previously mentioned, one of the main advantages stated for Fe-g-CN materials is the possibility of an *in situ* photo-Fenton reaction due to the reduction of dissolved oxygen into H_2O_2 by e^-_{CB} from the g-CN. Noteworthy, due to the low hole scavenger concentration (100 μM in this case), the formation of H_2O_2 was negligible even in the case of g-CN (<30 μM), in agreement with previous works (Sciscenko et al., 2024a). Only when adding significant concentrations of hole scavenger (methanol 3 M), g-CN led to significant H_2O_2 formation (ca. 1500 μM h^{-1} production rate, see Fig. 1C). As expected, for the illuminated Fe-g–CN–(0.07) in the presence of methanol 3 M, the H_2O_2 concentration led to a maximum formation of 30 μM in 30 min, which remained constant for the 3 h of irradiation. The lack of H_2O_2 accumulation in the case of illuminated Fe-g–CN–(0.07) is related to the Fenton reaction, decomposing the H_2O_2 as soon as it is generated. On the contrary, in the case of g-CN, the H_2O_2 can be only decomposed by the photogenerated holes and by its direct photolysis by UVA light, which, based on the obtained results, are negligible compared to the contribution of the Fenton catalytic cycle when iron is incorporated.

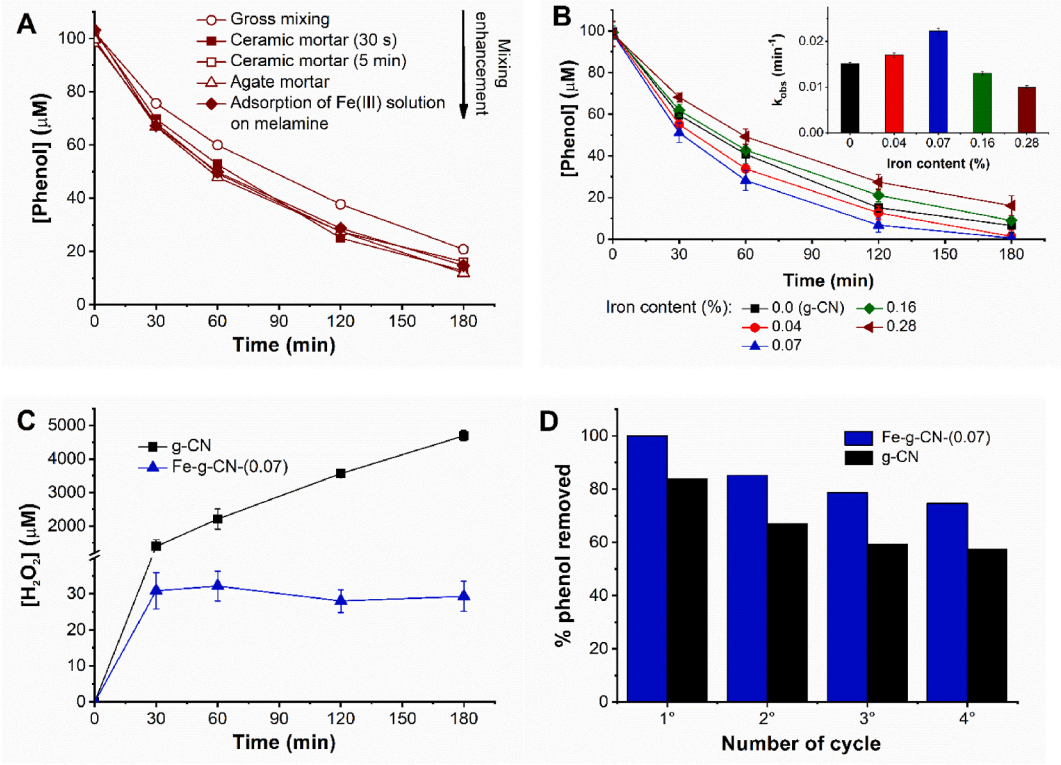

Fig. 1. (A) Starting iron/melamine mixing grade effect on photocatalytic efficiency of Fe-g–CN–(0.28). (B) Effect of iron content based on 100 μM phenol degradation under UVA irradiation; as inset, pseudo-first order kinetic rate constants. (C) H_2O_2 photo-generation under UVA irradiation when employing methanol 3 M as hole scavenger. (D) Percentage of phenol oxidation after 180 min with UVA irradiation during recycling test of g-CN and Fe-g–CN–(0.07). Conditions: $pH_0 = 7.0$ and 1.65 g L^{-1} of Fe-g–CN–(%Fe).

3.1.3. Reuse

The reusability of a catalyst could be the most relevant advantage with respect to homogeneous processes. Recycling tests for the photocatalyst in ultra-pure water matrix were also conducted under the same previous conditions described. At the end of every irradiation cycle, the catalyst was separated by centrifugation, the supernatant was removed and the remaining photocatalyst was reused in the subsequent cycle without further purification. Fig. 1D indicates that the performance of Fe-g-CN decreased with the number of applied cycles. We observed a reduction of ~20% in efficiency from the 1st to the 2nd irradiation cycle, while lower variations have been observed in the subsequent cycles of re-usage. An inherent contribution to phenol degradation efficiency decay also comes from photocatalyst loss after centrifugation-filtration process during each reuse; catalyst separation and reuse is a common drawback in heterogeneous photocatalysis-based AOPs especially with micrometric and nanometric catalysts (Rengifo-Herrera and Pulgarin, 2023). Similar results were observed for g-CN, observing 80% phenol degradation in the first cycle, and constantly reduced after each reutilization, reaching 60% degradation in the fourth cycle. To better emphasise the effect of catalyst loss in the recycling, analogous experiments were carried out without light irradiation (phenol removal by adsorption), observing a similar trend (shown in Fig. S1). These results suggest that the loss of catalyst should be the main contributor to the lower pollutant abatement with the recycling rather than its structural decomposition.

3.1.4. Iron leaching

The final concentration of dissolved total iron was negligible after 3 h of treatment in all cases (with or without UVA light irradiation), being below the technique's detection limit (0.1 mg L^{-1}), becoming detectable only with high iron loading materials, Fe-g–CN–(0.16) and Fe-g–CN–(0.28), where, noteworthy, the final total iron concentrations not exceeded the 0.5 mg L^{-1}, highlighting that iron was strongly attached within the g-CN honeycomb structure, in line with other works (Asif et al., 2023; Luo et al., 2016). To further verify that the iron leaching was not underestimated due to the plausible elimination of iron oxides with the sample filtration, an acidification with HCl 0.1 M was carried out shortly before filtration. In this way, the iron oxides should have been dissolved, not being retained together with the catalyst in the filter. Since we did not observe significant differences with the iron measurement with or without the acidification, we conclude that the iron leaching is, indeed, low. In agreement with these results, the material with the highest iron content, Fe-g–CN–(0.28), was left for 10 h agitation in HCl 0.01 M solution in order to enhance the iron leaching; noteworthy, the final iron concentration in solution still remained ca. 0.5 mg L^{-1}, which is only 4.5% respect to the total iron in the aqueous suspension (see Table S2 the measured iron content in each of the synthesised materials).

3.2. Effect of H_2O_2 addition

The material which gave the fastest phenol oxidation rates, Fe-g–CN–(0.07), was the chosen material to continue with along the work, comparing its efficiency towards pollutant abatement against g-CN.

As previously mentioned, since illuminated g-CN is able to photoproduce significative H_2O_2 only in the presence of a high concentration of hole scavengers (Fig. 1C), for the solutions of phenol 100 μM in ultra-pure water, we studied the effect of H_2O_2 addition at dark conditions (dark-Fenton evaluation) and in the presence of light (*in situ* and *ex situ* parallel photo-Fenton processes based on the generated and added H_2O_2, respectively).

If compared with other works, as detailed in the following subsections, the phenol removal rate by Fe-g–CN–(0.07) seemed lower than usual reported values for other target pollutants (ca. $k = 0.09$ min^{-1}), although high concentrations of H_2O_2 (ca. 200 mM) and dyes (methylene blue, for example) were here employed (Bicalho et al., 2017; Wang and Nan, 2020), which might explain the differences with literature. However, one must bear in mind that kinetic rate constants are strongly dependent on the dimensions of the reactor system, hence, their comparison with those obtained in analogous works being only useful in general terms.

3.2.1. Heterogeneous dark-Fenton

The dark-Fenton performance with Fe-g–CN–(0.07) was first evaluated, observing that only with H_2O_2 concentrations ≥5 mM the phenol degradation became noticeable after 3 h of treatment, being of 17% when employing 25 mM of H_2O_2 (see Fig. S2). Despite the poor performance towards phenol degradation in dark conditions with Fe-g–CN–(0.07), it was observed that H_2O_2 consumption was considerable in all cases (e.g., 70% after 3 h in the case of H_2O_2 1 mM). These results indicate that, although the Fe-g–CN–(0.07) should catalyse H_2O_2 decomposition, the generated reactive species (RS, the plausible FeO^{2+} and ROS) might attack the aromatic rings of g-CN rather than the phenol (Xiao et al., 2017), explaining the scarce removal of the latter. Furthermore, when repeating the experiments at pH 3.0 (optimal for homogeneous Fenton reaction, (Sciscenko et al., 2024b)), analogous results to that at pH 7 were obtained, indicating that the heterogeneous catalysis is predominating in the overall degradation process and that the AOP is scarcely pH-dependent. As expected, the combination of g-CN with H_2O_2 0–25 mM did not produce neither phenol nor H_2O_2 concentration abatements.

Finally, to discard contributions from homogeneous Fenton, experiments were driven employing 0.1 mg L^{-1} of Fe(III) (simulating the maximum iron which can eventually be leached from Fe-g–CN–(0.07)) in the presence of H_2O_2 1–25 mM. No appreciable phenol degradation was observed in at least 3 h (<1%), which was expected since homogeneous Fenton is inefficient at neutral pH conditions due to the fast precipitation of iron oxides and rapid Fe(II) oxidation by dissolved oxygen (Sciscenko et al., 2024b).

3.2.2. Heterogeneous photo-Fenton

As shown in Fig. 2A, similarly as with dark-Fenton results, under irradiation, although considerably faster H_2O_2 consumptions were obtained by Fe-g–CN–(0.07) compared with g-CN ($k_{Fe\text{-}g\text{-}CN\text{-}(0.07)} = 8.02 \times 10^{-2}$ min^{-1} and $k_{g\text{-}CN} = 2.83 \times 10^{-2}$ min^{-1}, respectively), slower phenol degradations were obtained with the former ($k_{g\text{-}CN} = 3.67 \times 10^{-2}$ min^{-1}; $k_{Fe\text{-}g\text{-}CN\text{-}(0.07)} = 1.68 \times 10^{-2}$ min^{-1}). These results were (at a certain point) counterintuitive since, despite the fact that an evident catalytic H_2O_2 decomposition was obtained, the likelihood higher reactive radicals production by Fe-g–CN–(0.07) did not increase the phenol removal rate. Similar results were also observed when changing the target pollutant to sulfamethoxazole (see Fig. S3), demonstrating independence from the chosen probe.

When comparing the kinetic rate constants of phenol oxidation obtained in absence and presence of H_2O_2 with the prepared Fe-g–CN–(% Fe), it was observed that as soon as iron is incorporated within the g-CN, a marked hindering effect by H_2O_2 1 mM addition was obtained, being the minimal with Fe-g–CN–(0.07), and closed to the unity for Fe-g–CN–(0.28) (see Fig. 2B). Therefore, the addition of external H_2O_2 reduces the photocatalytic degradation in these materials, only improved (i.e., no positive nor negative effect observed) with an iron excess. These observations can be explained by the fact that the generated RS should oxidise the g-CN structure rather than the target contaminant, in line with the discussion from the previous section, reducing their photocatalytic activity.

The phenol oxidation was only enhanced when an excess of reactive species was generated (i.e., able to oxidise the g-CN internal structure as well as the target pollutant), presumably because a fraction of the generated RS are able to diffuse from the neighbour of the iron-based catalytic sites to the bulk solution where they can react with the target compounds. To verify this hypothesis, the H_2O_2 initial concentration was increased from 1 to 25 mM (Fig. 2C), observing a phenol oxidation

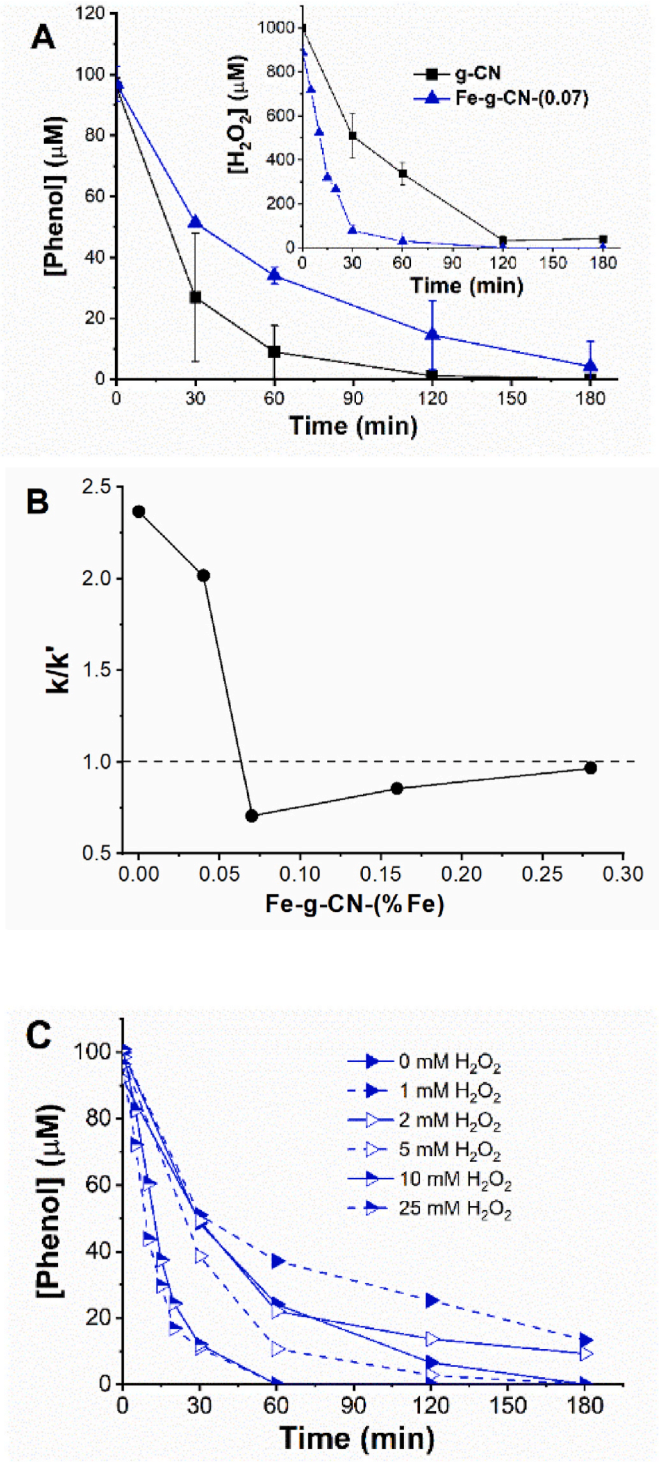

Fig. 2. (A) Phenol degradation and H_2O_2 kinetics (as inset) by illuminated g-CN and Fe-g–CN–(0.07) in the presence of H_2O_2 1 mM, (B) pseudo-first-order kinetic rate constants ratio in the UVA irradiated system with and without H_2O_2 1 mM (k and k', respectively) as a function of Fe percentage, and (C) effect of different H_2O_2 concentrations on phenol degradation by UVA/Fe-g–CN–(0.07).

enhancement, passing from a $k_{obs} = 1.02 \times 10^{-2}$ min^{-1} obtained with H_2O_2 1 mM, to 6.88×10^{-2} min^{-1} with H_2O_2 10 mM, rates comparable to those from other works (Goldstein et al., 2007; Torres-Pinto et al., 2020).

In Figs. S4A–B, the H_2O_2 decomposition kinetics by UVA/Fe-g–CN–(0.07) and UVA are shown, respectively, observing a several-order faster concentration decay in the presence of the photocatalyst than in its absence (<30% by UVA light alone in 2 h, being >99% in the same period when the photocatalyst was present). Finally, as exhibited in Fig. S4C (phenol oxidation by UVA/H_2O_2), the $HO^\bullet$ coming from H_2O_2 direct photolysis should also contribute to the overall phenol oxidation (becoming more relevant for H_2O_2 concentrations higher than 1 mM). When adding Fe(III) 0.1 mg L^{-1} to the latter (in order to determine the contribution from homogeneous photo-Fenton) no significative differences were observed respect to UVA/H_2O_2 in line with the literature (Buitrago et al., 2020; Serra-Clusellas et al., 2018; Vallés et al., 2023).

These results indicate that a 5–10 mM concentration of H_2O_2 is needed to start observing the photo-Fenton enhancement, which is in line with the degradation constant obtained at high concentrations (15–100 mM) usually reported in similar works with visible light (An et al., 2018; Li et al., 2021; Shi et al., 2024).

3.3. Detection of reactive species and catalytic degradation mechanisms

The absence of an increase in phenol degradation for concentrations ≤5 mM of H_2O_2 gave indications that produced RS followed a different fate instead of the oxidation of the target pollutant. To determine the fate of the RS produced (and the possible mechanisms of phenol degradation involved in the presence of Fe-g–CN–(%Fe)), studies were carried out by using selective scavengers, EPR, and the characterisation of the materials (the latter described in section 3.5).

The graph in Fig. 3A summarises the effect of 200 μM scavenger additions. Only p-BQ produced a considerable hindering effect on phenol oxidation (21.2% of phenol removal in 3 h, compared with >90% in the absence of scavengers in the same period), being scarce in the presence of FFA, and negligible when IPA or DMSO were added. These results suggest that $HO_2^\bullet$ might be the major RS contributing to phenol oxidation rather than $^1O_2$, $HO^\bullet$, or FeO^{2+}, in line with other works (Velo-Gala et al., 2021). However, although p-BQ is the most used quencher to determine the effect of superoxide radicals, it is usually added under dark conditions or with visible light irradiation. As reported in Fig. S5A, p-BQ may partially act as a UV irradiation filter, reducing the total radiance available to the photocatalyst, as well as it also undergoes to hydroquinone through its photolytic degradation (see Fig. S6), the latter being more reactive against h^+_{VB} or RS than phenol as it has the double hydroxyl groups (Józsa et al., 2018). Other works also reported a possible reactivity of p-BQ with the e^-_{CB} and $HO^\bullet$ (Fónagy et al., 2021; Pelaez et al., 2016), not guaranteeing optimal selectivity of p-BQ for the $HO_2^\bullet$ quenching. Based on these arguments, the results from p-BQ can easily lead to misinterpretations (Schneider et al., 2020).

To gain further insights into the role of ROS, the phenol degradation by UVA/Fe-g–CN–0.07 was performed under anaerobic conditions, observing slower removals ($k_{OBS} = 1.31 \times 10^{-2}$ min^{-1}, see Fig. 3B). These results support the hypothesis of $HO_2^\bullet$ as the ROS responsible for phenol oxidation. On the other hand, regarding the plausible role of $HO^\bullet$ on phenol oxidation, an additional experiment with a higher IPA concentration (800 μM) was performed, observing a slight scavenging of 5% respect to the phenol kinetics without scavenger addition, therefore, with no significant differences with one and the other. A negligible effect was also observed when changing the probe to iodide (h^+_{VB} scavenger (Schneider et al., 2020)) 200 and 800 μM observing only 3% hindering, respectively. These results support the idea that rather than h^+_{VB} or $HO^\bullet$, $HO_2^\bullet$ was the main responsible for phenol oxidation.

Finally, the EPR analysis indicated that ROS were not generated significantly, observing small signals corresponding to DMPO-OH, and negligible of DMPO-OOH nor TEMP-O (see Fig. 3C and D). Although these observations might be opposed to most works demonstrating clear and intense signals of the aforementioned ROS (Feng et al., 2024; Shi et al., 2024), as previously discussed, they all employed high (and unviable from a large-scale point of view) H_2O_2 concentrations respect to the 1 mM here used. Therefore, as hypothesised in previous sections, the generated ROS mostly oxidise the g-CN structure (more abundant and

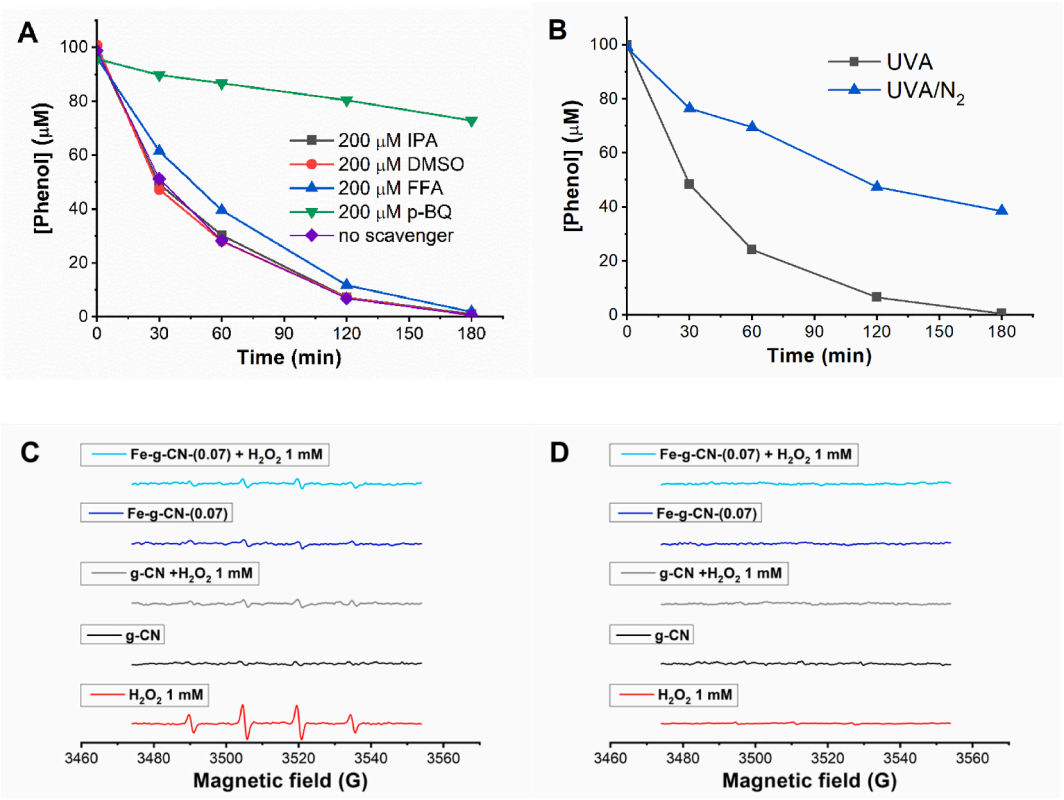

Fig. 3. (A) Addition of 200 μM scavengers (IPA, DMSO, FFA, and p-BQ) effect on photocatalytic degradation of phenol by Fe-g–CN–(0.07). B) Contribution of anaerobic conditions on UVA photocatalytic degradation of phenol by Fe-g–CN–(0.07). (C) EPR results for $^{\bullet}OH$ and $HO_2^{\bullet}$ detection with DMPO and (D) for $^1O_2$ with TEMP after 15 min of irradiation experiments.

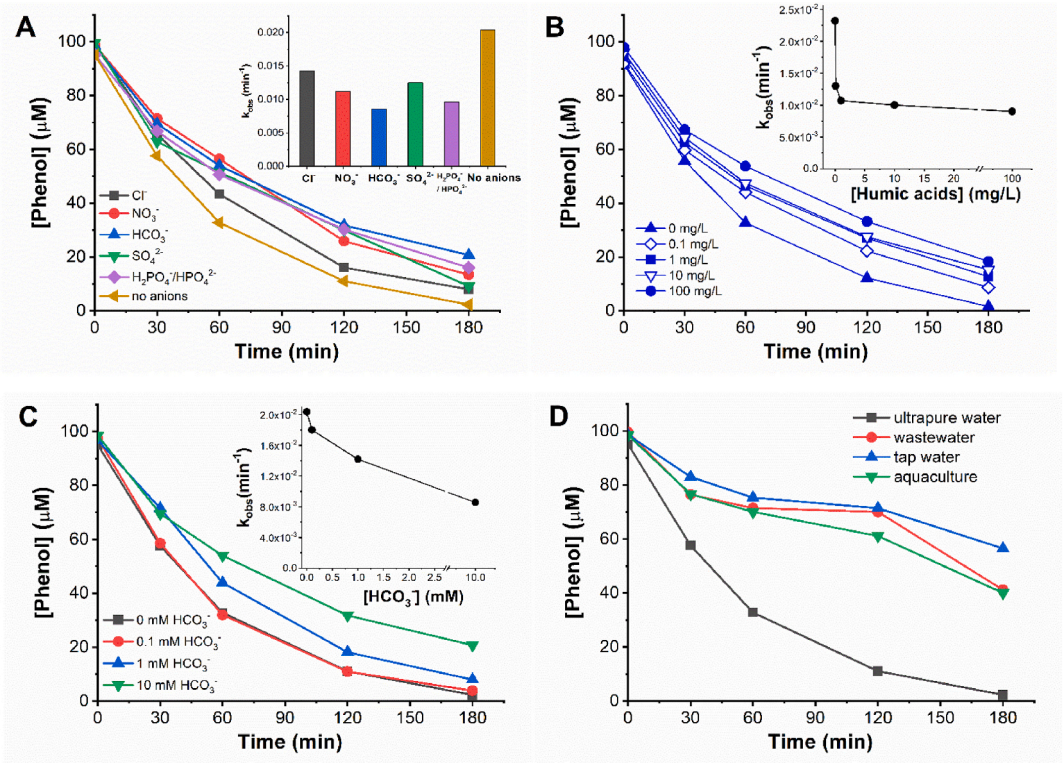

Fig. 4. Influence of (A) 10 mM main anions (Cl^-, NO_3^-, HCO_3^-, SO_4^{2-}, $H_2PO_4^-$), (B) increasing concentrations of humic acids (0–100 mg L^{-1}), (C) increasing concentration of HCO_3^- (0–10 mM), (D) real matrix on the photochemical Fe-g–CN–(0.07) performance.

requiring a lower diffusion-controlled rate than the target pollutant) than the spin traps.

3.4. Effect of water constituents and application in real water matrices

Analyses were conducted to determine the contribution of the main organic and inorganic components in the water on the performance of the Fe-g–CN–(0.07). Regarding anions (Fig. 4A), no significative hindering effect was observed, in spite of their high concentration here employed (10 mM each) with respect to frequent concentrations found in natural water bodies or wastewater treatment plants' effluents. Overall, except for Cl^-, with negligible scavenging effect, all the other anions (HCO_3^-, NO_3^-, SO_4^{2-}, $H_2PO_4^-$) produced a similar hindering effect, reducing the phenol kinetic rate constant to ca. 1×10^{-2} min^{-1}, only the half with respect to the system in the absence of anions. These results are in line with the observations stating that the generated RS would rather oxidise the g-CN internal structure than the phenol itself and demonstrate a good efficiency of the synthesised photocatalyst also in the presence of high anion concentrations.

Conversely, the presence of humic acids had a considerable influence on the performance of the photocatalyst, the hindering effect being evident with concentrations as low as 0.1 mg L^{-1} and remaining relatively constant despite variations in concentration by up to three orders of magnitude (see Fig. 4B), most likely due to the competition for the h^+_{VB} and $HO_2^{\bullet}$ with phenol and the associated screening effect, reducing the photon flux arriving to the photocatalyst (see humic acid absorbance spectra shown in Fig. S5B). Therefore, differently from anions, dissolved organic matter should represent a serious interference for Fe-g-CN materials, which is in line with other works obtaining analogous results (Ding et al., 2015; Xue et al., 2020). Fig. 4C shows as an example the kinetic rate constants decrease with increasing HCO_3^- concentration.

Finally, the heterogeneous photo-Fenton treatment was studied towards the degradation of phenol in three real aqueous matrices: tap water, water from an aquaculture system, and wastewater primary treatment effluent. The trends depicted in Fig. 4D indicate a maximum phenol reduction of 50% after 3 h of irradiation in real water matrices compared with complete removal in ultra-pure water. The photocatalyst performance was nearly identical in tap water, wastewater or aquaculture matrices, in line with their TOC content and/or anion concentrations (see Table S1).

3.5. Characterization of Fe-g–CN–(%Fe)

The characterisation of g-CN (without iron) was in agreement with those published in a previous work indicating the predominance of melon (Sciscenko et al., 2024a): i) C:N and H:C ratios of 0.671 ± 0.001 and 0.62 ± 0.01, respectively; ii) diffuse reflectance absorption with band gap transition at ~450 nm; iii) FT-IR/ATR with stretching and deformation modes of –NH and $–NH_2$ groups (3000–3500 cm^{-1}), and signals within 1200–1650 cm^{-1} range corresponding to the typical stretching modes of C–N heterocycles; iv) XRD diffraction wide peaks at 2θ = 12–15° ((100) in-plane structural motif) and 25–30° ((002) stacking of polymeric sheets). The incorporation of iron slightly changed the aforementioned properties (see Fig. 5), in agreement with the vast literature on the matter, indicating the good dispersion of iron within the g-CN structure (Bicalho et al., 2017; Li et al., 2007; Xu et al., 2015). Moreover, the reported amounts of iron were scarce, thus, insignificant changes in characterisation measurements were also expected. For instance, according to the total iron determination on Fe-g–CN–(%Fe) materials (see Table S2), the Fe-g–CN–(0.07) had 0.17% Fe w/w. The iron content in the photocatalyst was 1.8 times more than that in the initial mixture with melamine (see Fig. S7B), indicating that the melamine sublimation and the g-CN thermal decomposition are not affected by the iron loadings (Bicalho et al., 2017).

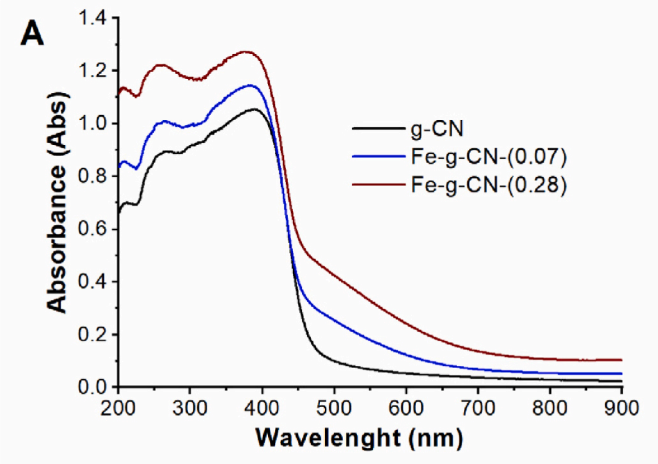

Fig. 5. Characterisation of g-CN and Fe-g–CN–(%Fe) with: A) diffuse reflectance analysis, B) FT-IR/ATR and C) XRD.

3.5.1. Proving the higher oxidation of g-CN structure when iron is incorporated

To prove the hypothesis of carbon nitride oxidation by generated RS, g-CN and Fe-g–CN–(0.07) were characterised after the UVA irradiation in the absence and the presence of initial H_2O_2 10 mM by measuring the FT-IR/ATR, XRD, and formed NO_3^- as a potential product of g-CN

mineralization, respectively. In order to do so, the photocatalysts of the irradiated solutions were recovered by filtration, dried in an oven at 60 °C, and subjected to the chosen measurements (FT-IR/ATR and XRD), whereas the resulting filtered water was afterwards analysed by ionic chromatography.

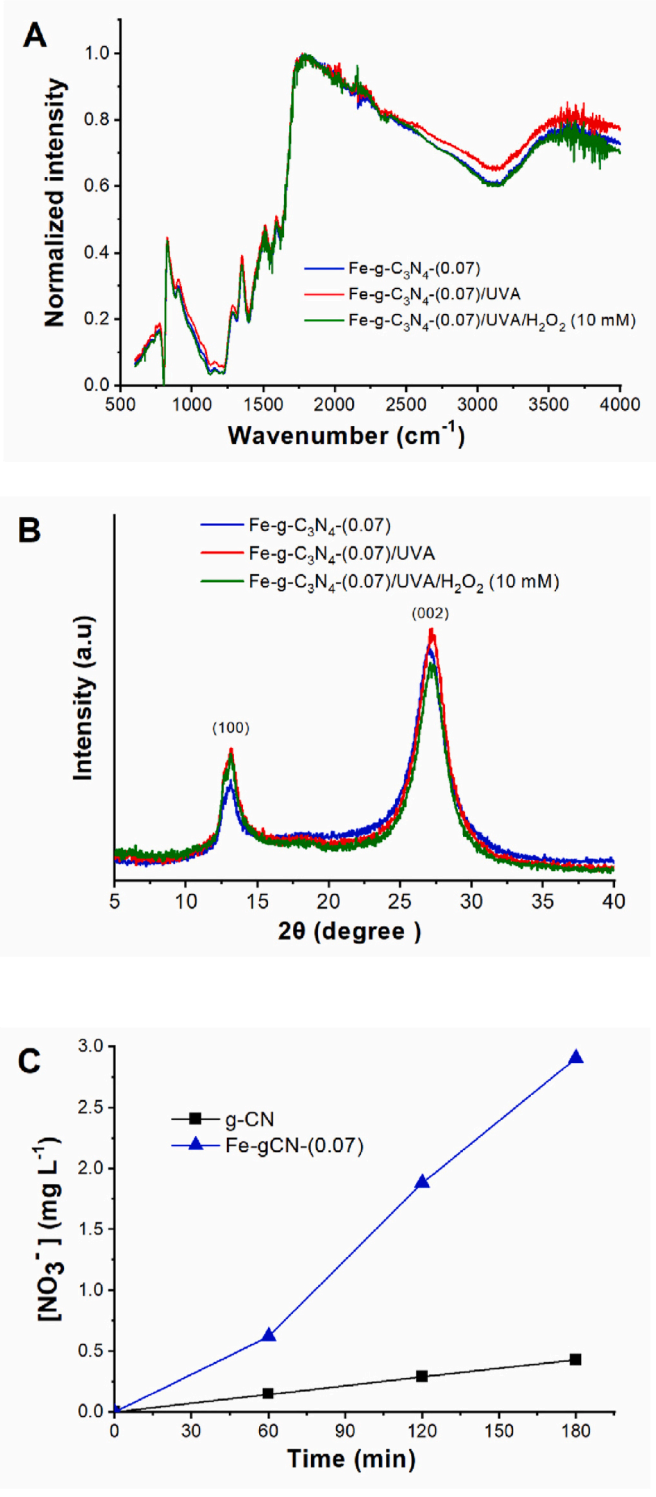

Fig. 6. A) FT-IR/ATR spectra of Fe-g–CN–(0.07) before and after irradiation experiments, with and without H_2O_2 10 mM additions. B) Fe-g–CN–(0.07) diffractograms before and after irradiation experiments, with and without 10 mM H_2O_2 additions. C) Concentration of NO_3^- with time by illuminated g-CN and Fe-g–CN–0.07 in presence of H_2O_2 10 mM.

Based on the obtained results, FT-IR/ATR did not show significant changes in the Fe-g-CN structure, as shown in Fig. 6A, where even at high H_2O_2 concentrations (10 mM), negligible variations were observed with respect to the starting material. No significative differences were neither observed in the diffractograms (Fig. 6B), the signals being observed at analogous 2θ values and conserving the same width, indicating that the crystallinity of the material was conserved. Analogous results were observed for g-CN, the FT-IR/ATR and XRD results not changing significantly after the UVA and UVA/H_2O_2 processes. On the contrary, the formed NO_3^- evidenced the higher degradation of g-CN when iron is incorporated (when the photo-Fenton process occurs) compared to the case of g-CN alone. As shown in Fig. 6C, illuminated Fe-g–CN–(0.07) in the presence of H_2O_2 10 mM systems lead to 6 times more NO_3^- formation (16 μM h^{-1}) than g-CN (2.5 μM h^{-1}). Although less marked, this difference was also evidenced in the absence of H_2O_2 (see Fig. S8).

The higher NO_3^- formation by Fe-g–CN–(0.07) compared to g-CN confirms our hypothesis that the formed RS by the photo-Fenton process oxidise the carbon nitride structure rather than the target pollutant, in line with the results exhibited in the previous sections. These results are also in line with other works reporting g-CN self-degradation when more oxidising conditions are employed (Hasabeldaim et al., 2023; Li et al., 2023; Xiao et al., 2017). Interestingly, similar conclusions have been reported in photo-Fenton processes based on Fe(III)-EDDS (ethylenediamine-N,N'-disuccinic acid) complex and soybean peroxidase, where the reactive species catalytically formed during the H_2O_2 decomposition at the enzymatic site of the peroxidase were not able to escape from the solvent cage of the enzyme and did not react with the target pollutant (Bertolotti et al., 2022).

4. Conclusions

This work reported that the incorporation of iron within g-CN reduces its stability, enhancing its structural decomposition, supplementing the missing knowledge on the matter in the literature. Results demonstrated that, since the Fe-g-CN could lead to a higher generation of RS (e.g., $HO_2^{\bullet}$, $HO^{\bullet}$, $^1O_2$ or FeO^{2+}) due to the heterogeneous photo-Fenton process, these mostly react with the photocatalyst structure rather than with the emerging contaminants, evidenced by a decay of the photocatalytic activity in the presence of external H_2O_2 addition and the higher release of nitrates compared to g-CN. Therefore, although some authors report Fe-g-CN as a promising material to drive heterogeneous photo-Fenton processes, we believe that it might have more drawbacks than advantages. These results also explain the reason of the usually reported high H_2O_2 concentrations (≥25 mM) required to observe some contaminant removal by heterogeneous dark-Fenton process with Fe-g-CN materials. Further studies monitoring the NO_3^- release over time, as well as an organic carbon increment due to the release of g-CN oxidation by-products, are required in future works to better asses the hazards associated with water treatment by carbon nitride materials.

The other aspects of the work explained why small amounts of iron (<0.17% w/w in g-CN) improve the oxidative performance of illuminated g-CN as well as the reasons for choosing a simple grinding between the precursors ($FeCl_3$ and melamine in this case). Regarding the reactive species involved in the pollutant abatement, our results suggest that rather than h_{VB}^+ or $HO^{\bullet}$, $HO_2^{\bullet}$ should be the one that produces the contaminant removal.

CRediT authorship contribution statement

Simone Pellegrino: Writing – original draft, Methodology, Investigation, Formal analysis, Data curation, Conceptualization. **Iván Sciscenko:** Writing – review & editing, Writing – original draft, Visualization, Validation, Supervision, Project administration, Methodology, Investigation, Funding acquisition, Formal analysis, Data

curation, Conceptualization. **Fabrizio Caldera:** Writing – review & editing, Formal analysis. **Claudio Minero:** Writing – review & editing, Resources. **Enzo Laurenti:** Writing – review & editing, Validation, Resources, Formal analysis. **Marco Minella:** Writing – review & editing, Visualization, Validation, Supervision, Resources, Project administration, Funding acquisition, Conceptualization.

Declaration of competing interest

The authors declare that they have no known competing financial interests or personal relationships that could have appeared to influence the work reported in this paper.

Acknowledgements

The authors acknowledge support from the Project CH4.0 under the MUR program "Dipartimenti di Eccellenza 2023–2027 (CUP: D13C2200352001)". I. Sciscenko wants to acknowledge to Generalitat Valenciana, CIAPOS 2021/311, project SANITISE, and the Horizon Europe research and innovation program, Marie Skłodowska-Curie Actions PF grant agreement No 101146398 (HERO4PFAS project), for the funding.

Appendix A. Supplementary data

Supplementary data to this article can be found online at https://doi.org/10.1016/j.chemosphere.2025.144255.

Data availability

Data will be made available on request.

References

An, S., Zhang, G., Wang, T., Zhang, W., Li, K., Song, C., Miller, J.T., Miao, S., Wang, J., Guo, X., 2018. High-density ultra-small clusters and single-atom Fe sites embedded in graphitic carbon nitride (g-C_3N_4) for highly efficient catalytic advanced oxidation processes. ACS Nano 12, 9441–9450. https://doi.org/10.1021/acsnano.8b04693.

Appiani, E., Ossola, R., Latch, D.E., Erickson, P.R., McNeill, K., 2017. Aqueous singlet oxygen reaction kinetics of furfuryl alcohol: effect of temperature, pH, and salt content. Environ. Sci. Process. Impacts 19, 507–516. https://doi.org/10.1039/c6em00646a.

Asif, A.H., Rafique, N., Hirani, R.A.K., Shi, L., Zhang, S., Wang, S., Sun, H., 2023. Graphitic carbon nitride engineered α-Fe_2O_3/rGO heterostructure for visible-light-driven photochemical oxidation of sulfamethoxazole. Chem. Eng. J. 451, 138630. https://doi.org/10.1016/j.cej.2022.138630.

Ben-Refael, A., Benisti, I., Paz, Y., 2020. Transient photoinduced phenomena in graphitic carbon nitride as measured at nanoseconds resolution by step-scan FTIR. Catal. Today 340, 97–105. https://doi.org/10.1016/j.cattod.2018.11.010.

Bertolotti, S., Minella, M., Laurenti, E., Brigante, M., Mailhot, G., Bianco Prevot, A., 2022. Application of Fe(III)–EDDS complexes and soybean peroxidase in photo-Fenton processes for organic pollutant removal: insights into possible synergistic effects. Photochem. Photobiol. Sci. 22, 603–613. https://doi.org/10.1007/s43630-022-00339-4.

Bicalho, H.A., Lopez, J.L., Binatti, I., Batista, P.F.R., Ardisson, J.D., Resende, R.R., Lorençon, E., 2017. Facile synthesis of highly dispersed Fe(II)-doped g-C_3N_4 and its application in Fenton-like catalysis. Mol. Catal. 435, 156–165. https://doi.org/10.1016/j.mcat.2017.04.003.

Buitrago, J.L., Sanabria, J., Gútierrez-Zapata, H.M., Urbano-Ceron, F.J., García-Barco, A., Osorio-Vargas, P., Rengifo-Herrera, J.A., 2020. Photo-Fenton process at natural conditions of pH, iron, ions, and humic acids for degradation of diuron and amoxicillin. Environ. Sci. Pollut. Res. 27, 1608–1624. https://doi.org/10.1007/s11356-019-06700-y.

Buxton, G.V., Greenstock, C.L., Helman, W.P., Ross, A.B., 1988. Critical Review of rate constants for reactions of hydrated electrons, hydrogen atoms and hydroxyl radicals ($^{\bullet}OH/^{\bullet}O^{-}$ in Aqueous Solution. J. Phys. Chem. Ref. Data 17, 513–886. https://doi.org/10.1063/1.555805.

Cai, L., Yao, Q., Du, X., Tao, X., Zou, M., Zhou, J., Dang, Z., Lu, G., 2024. Identification of superoxide contribution through the quenching method and model system. ACS ES&T Eng. 4, 2145–2154. https://doi.org/10.1021/acsestengg.4c00187.

Chen, Z., Yan, Y., Lu, C., Lin, X., Fu, Z., Shi, W., Guo, F., 2023. Photocatalytic self-Fenton system of g-C_3N_4-based for degradation of emerging contaminants: a review of advances and prospects. Molecules 28, 5916. https://doi.org/10.3390/molecules28155916.

Christou, A., Beretsou, V.G., Iakovides, I.C., Karaolia, P., Michael, C., Benmarhnia, T., Chefetz, B., Donner, E., Gawlik, B.M., Lee, Y., Lim, T.T., Lundy, L., Maffettone, R., Rizzo, L., Topp, E., Fatta-Kassinos, D., 2024. Sustainable wastewater reuse for agriculture. Nat. Rev. Earth Environ. 5, 504–521. https://doi.org/10.1038/s43017-024-00560-y.

Coha, M., Farinelli, G., Tiraferri, A., Minella, M., Vione, D., 2021. Advanced oxidation processes in the removal of organic substances from produced water: potential, configurations, and research needs. Chem. Eng. J. 414, 128668. https://doi.org/10.1016/j.cej.2021.128668.

Ding, C., Kang, S., Li, W., Gao, W., Zhang, Z., Zheng, L., Cui, L., 2022. Mesoporous structure and amorphous Fe-N sites regulation in Fe-g-C_3N_4 for boosted visible-light-driven photo-Fenton reaction. J. Colloid Interface Sci. 608, 2515–2528. https://doi.org/10.1016/j.jcis.2021.10.168.

Ding, S.L., Wang, X.K., Jiang, W.Q., Zhao, R.S., Shen, T.T., Wang, C., Wang, X., 2015. Influence of pH, inorganic anions, and dissolved organic matter on the photolysis of antimicrobial triclocarban in aqueous systems under simulated sunlight irradiation. Environ. Sci. Pollut. Control Ser. 22, 5204–5211. https://doi.org/10.1007/s11356-014-3686-x.

Fei, J., Peng, X., Jiang, L., Yuan, X., Chen, X., Zhao, Y., Zhang, W., 2021. Recent advances in graphitic carbon nitride as a catalyst for heterogeneous Fenton-like reactions. Dalton Trans. 50, 16887–16908. https://doi.org/10.1039/d1dt02367e.

Feng, Y., Liang, Y., Ding, C., Jiang, Y., Jin, H., Rong, S., Wu, J., He, S., Xia, C., Xue, L., 2024. Sustainable design of photo-Fenton-like oxidation process in actual livestock wastewater through the highly dispersed $FeCl_3$ anchoring on a g-C_3N_4 substrate. Water Res. 259, 121889. https://doi.org/10.1016/j.watres.2024.121889.

Fónagy, O., Szabó-Bárdos, E., Horváth, O., 2021. 1,4-Benzoquinone and 1,4-hydroquinone based determination of electron and superoxide radical formed in heterogeneous photocatalytic systems. J. Photochem. Photobiol. Chem. 407, 113057. https://doi.org/10.1016/j.jphotochem.2020.113057.

Goldstein, S., Aschengrau, D., Diamant, Y., Rabani, J., 2007. Photolysis of aqueous H_2O_2: quantum yield and applications for polychromatic UV actinometry in photoreactors. Environ. Sci. Technol. 41, 7486–7490. https://doi.org/10.1021/es071379t.

Haider, Z., Cho, H., Moon, G. hee, Kim, H. il, 2019. Minireview: selective production of hydrogen peroxide as a clean oxidant over structurally tailored carbon nitride photocatalysts. Catal. Today 335, 55–64. https://doi.org/10.1016/j.cattod.2018.11.067.

Hasabeldaim, E.H.H., Swart, H.C., Coetsee, E., Kumar, P., Kroon, R.E., 2023. Degradation and chemical stability of graphitic carbon nitride during ultraviolet light irradiation. Mater. Chem. Phys. 308, 128252. https://doi.org/10.1016/j.matchemphys.2023.128252.

Józsa, É., Kiss, V., Ősz, K., 2018. Photochemical processes of 1,4-benzoquinones in aqueous medium. J. Photochem. Photobiol. Chem. 360, 166–173. https://doi.org/10.1016/j.jphotochem.2018.04.024.

Lau, V.W.H., Mesch, M.B., Duppel, V., Blum, V., Senker, J., Lotsch, B.V., 2015. Low-molecular-weight carbon nitrides for solar hydrogen evolution. J. Am. Chem. Soc. 137, 1064–1072. https://doi.org/10.1021/ja511802c.

Lei, G., Zhao, W., Shen, L., Liang, S., Au, C., Jiang, L., 2020. Isolated iron sites embedded in graphitic carbon nitride (g-C_3N_4) for efficient oxidative desulfurization. Appl. Catal. B Environ. 267, 118663. https://doi.org/10.1016/j.apcatb.2020.118663.

Li, C., Yang, X., Yang, B., Yan, Y., Qian, Y., 2007. Synthesis and characterization of nitrogen-rich graphitic carbon nitride. Mater. Chem. Phys. 103, 427–432. https://doi.org/10.1016/j.matchemphys.2007.02.057.

Li, K., Liang, Y., Yang, H., An, S., Shi, H., Song, C., Guo, X., 2021. New insight into the mechanism of enhanced photo-Fenton reaction efficiency for Fe-doped semiconductors: a case study of Fe/g-C_3N_4. Catal. Today 371, 58–63. https://doi.org/10.1016/j.cattod.2020.07.026.

Li, M., Durkin, D.P., Waller, G., Yu, Y., Men, Y., Ye, T., Chen, H., Shuai, D., 2023. Transformation of graphitic carbon nitride by reactive chlorine species: "weak" oxidants are the main players. Environ. Sci. Technol. 57, 2749–2757. https://doi.org/10.1021/acs.est.2c06381.

Lin, J., Tian, W., Guan, Z., Zhang, H., Duan, X., Wang, H., Sun, H., Fang, Y., Huang, Y., Wang, S., 2022. Functional carbon nitride materials in photo-Fenton-like catalysis for environmental remediation. Adv. Funct. Mater. 32, 2201743. https://doi.org/10.1002/adfm.202201743.

Lotsch, B.V., Schnick, W., 2005. Thermal conversion of guanylurea dicyanamide into graphitic carbon nitride via prototype CNx precursors. Chem. Mater. 17, 3976–3982. https://doi.org/10.1021/cm050350q.

Luo, L., Zhang, A., Janik, M.J., Song, C., Guo, X., 2016. Mesoporous graphitic carbon nitride functionalized iron oxides for promoting phenol oxidation activity. RSC Adv. 6, 91960–91967. https://doi.org/10.1039/c6ra19455a.

Luo, W., Huang, W., Feng, X., Huang, Y., Song, X., Lin, H., Wang, S., Mailhot, G., 2020. The utilization of Fe-doped g-C_3N_4 in a heterogeneous photo-Fenton-like catalytic system: the effect of different parameters and a system mechanism investigation. RSC Adv. 10, 21876–21886. https://doi.org/10.1039/d0ra00993h.

Mao, S., Liu, C., Wu, Y., Xia, M., Wang, F., 2022. Porous P, Fe-doped g-C_3N_4 nanostructure with enhanced photo-Fenton activity for removal of tetracycline hydrochloride: mechanism insight, DFT calculation and degradation pathways. Chemosphere 291, 133039. https://doi.org/10.1016/j.chemosphere.2021.133039.

Miklos, D.B., Remy, C., Jekel, M., Linden, K.G., Drewes, J.E., Hübner, U., 2018. Evaluation of advanced oxidation processes for water and wastewater treatment – a critical review. Water Res. 139, 118–131. https://doi.org/10.1016/j.watres.2018.03.042.

Minella, M., Sordello, F., Minero, C., 2021. Graphitic carbon nitride-based metal-free photocatalyst. In: Materials Science in Photocatalysis. Elsevier, pp. 449–484. https://doi.org/10.1016/B978-0-12-821859-4.00025-8.

Pelaez, M., Falaras, P., Likodimos, V., O'Shea, K., de la Cruz, A.A., Dunlop, P.S.M., Byrne, J.A., Dionysiou, D.D., 2016. Use of selected scavengers for the determination of NF-TiO_2 reactive oxygen species during the degradation of microcystin-LR under

visible light irradiation. J. Mol. Catal. Chem. 425, 183–189. https://doi.org/10.1016/j.molcata.2016.09.035.
Pestovsky, O., Bakac, A., 2006. Aqueous ferryl(IV) ion: kinetics of oxygen atom transfer to substrates and oxo exchange with solvent water. Inorg. Chem. 45, 814–820. https://doi.org/10.1021/ic051868z.
Rengifo-Herrera, J.A., Pulgarin, C., 2023. Why five decades of massive research on heterogeneous photocatalysis, especially on TiO_2, has not yet driven to water disinfection and detoxification applications? Critical review of drawbacks and challenges. Chem. Eng. J. 477, 146875. https://doi.org/10.1016/j.cej.2023.146875.
Schneider, J.T., Firak, D.S., Ribeiro, R.R., Peralta-Zamora, P., 2020. Use of scavenger agents in heterogeneous photocatalysis: truths, half-truths, and misinterpretations. Phys. Chem. Chem. Phys. 22, 15723–15733. https://doi.org/10.1039/d0cp02411b.
Sciscenko, I., Actis, A., Salvadori, E., Arques, A., Minero, C., Sordello, F., Minella, M., 2024a. Ultraviolet-A light/oligomeric melem vs. visible light/graphitic carbon nitride towards H_2O_2 photo-production and pollutants degradation: sometimes less is more. J. Environ. Chem. Eng. 12, 114093. https://doi.org/10.1016/j.jece.2024.114093.
Sciscenko, I., Arques, A., Varga, Z., Bouchonnet, S., Monfort, O., Brigante, M., Mailhot, G., 2021. Significant role of iron on the fate and photodegradation of enrofloxacin. Chemosphere 270, 129791. https://doi.org/10.1016/j.chemosphere.2021.129791.
Sciscenko, I., Vione, D., Minella, M., 2024b. Infancy of peracetic acid activation by iron, a new Fenton-based process: a review. Heliyon 10, e27036. https://doi.org/10.1016/j.heliyon.2024.e27036.
Serra-Clusellas, A., De Angelis, L., Lin, C.H., Vo, P., Bayati, M., Sumner, L., Lei, Z., Amaral, N.B., Bertini, L.M., Mazza, J., Pizzio, L.R., Stripeikis, J.D., Rengifo-Herrera, J.A., Fidalgo de Cortalezzi, M.M., 2018. Abatement of 2,4-D by H_2O_2 solar photolysis and solar photo-Fenton-like process with minute Fe(III) concentrations. Water Res. 144, 572–580. https://doi.org/10.1016/j.watres.2018.07.072.
Shi, Y., Zhu, Q., Li, Y., Tao, Y., Li, K., Xu, K., Shang, H., Chen, M., Li, H., Zhang, D., Li, G., 2024. Low-coordinated Fe–N_3 sites in carbon nitride for efficient photo-Fenton wastewater treatment. Mater. Today Chem. 38, 102125. https://doi.org/10.1016/j.mtchem.2024.102125.
Torres-Pinto, A., Sampaio, M.J., Teixo, J., Silva, C.G., Faria, J.L., Silva, A.M.T., 2020. Photo-Fenton degradation assisted by in situ generation of hydrogen peroxide using a carbon nitride photocatalyst. J. Water Process Eng. 37, 101467. https://doi.org/10.1016/j.jwpe.2020.101467.
Vallés, I., Sciscenko, I., Mora, M., Micó, P., Amat, A.M., Santos-Juanes, L., Moreno-Andrés, J., Arques, A., 2023. On the relevant role of iron complexation for the performance of photo-Fenton process at mild pH: role of ring substitution in phenolic ligand and interaction with halides. Appl. Catal. B Environ. 331, 122708. https://doi.org/10.1016/j.apcatb.2023.122708.
Velo-Gala, I., Torres-Pinto, A., Silva, C.G., Ohtani, B., Silva, A.M.T., Faria, J.L., 2021. Graphitic carbon nitride photocatalysis: the hydroperoxyl radical role revealed by kinetic modelling. Catal. Sci. Technol. 11, 7712–7726. https://doi.org/10.1039/d1cy01657a.
Wang, X., Lu, W., Zhao, Z., Zhong, H., Zhu, Z., Chen, W., 2020. In situ stable growth of β-FeOOH on g-C_3N_4 for deep oxidation of emerging contaminants by photocatalytic activation of peroxymonosulfate under solar irradiation. Chem. Eng. J. 400, 125872. https://doi.org/10.1016/j.cej.2020.125872.
Wang, X., Nan, Z., 2020. Highly efficient Fenton-like catalyst Fe-g-C_3N_4 porous nanosheets formation and catalytic mechanism. Sep. Purif. Technol. 233, 116023. https://doi.org/10.1016/j.seppur.2019.116023.
Wang, Y.-D., Lee, T.-W., Lo, Y.-C., Hong, W.-J., Chen, C., 2021. Insights into photochemical stability of graphitic carbon nitride-based photocatalysts in water treatment. Carbon 175, 223–232. https://doi.org/10.1016/j.carbon.2020.12.074.
Xiao, J., Han, Q., Xie, Y., Yang, J., Su, Q., Chen, Y., Cao, H., 2017. Is C_3N_4 chemically stable toward reactive oxygen species in sunlight-driven water treatment? Environ. Sci. Technol. 51, 13380–13387. https://doi.org/10.1021/acs.est.7b04215.
Xu, J., Jiang, Q., Chen, T., Wu, F., Li, Y.X., 2015. Vanadia supported on mesoporous carbon nitride as a highly efficient catalyst for hydroxylation of benzene to phenol. Catal. Sci. Technol. 5, 1504–1513. https://doi.org/10.1039/c4cy01373e.
Xue, W., Cao, S., Liu, R., Tang, R., Chen, H., Jiang, F., 2020. Preparation of nitrogen-containing carbon using a one-step thermal polymerization method for activation of peroxymonosulfate to degrade bisphenol A. Chemosphere 248, 126053. https://doi.org/10.1016/j.chemosphere.2020.126053.
Yong, X.Y., Ji, Y.X., Yang, Q.W., Li, B., Cheng, X.L., Zhou, J., Zhang, X.Y., 2024. Fe-doped g-C_3N_4 with duel active sites for ultrafast degradation of organic pollutants via visible-light-driven photo-Fenton reaction: insight into the performance, kinetics, and mechanism. Chemosphere 351, 141135. https://doi.org/10.1016/j.chemosphere.2024.141135.
Zhou, B., Wang, J., Guo, Z., Tan, H., Zhu, X., 2006. A simple colorimetric method for determination of hydrogen peroxide in plant tissues. Plant Growth Regul. 49, 113–118. https://doi.org/10.1007/s10725-006-9000-2.
Zhu, J., Xiao, P., Li, H., Carabineiro, S.A.C., 2014. Graphitic carbon nitride: synthesis, properties, and applications in catalysis. ACS Appl. Mater. Interfaces 6, 16449–16465. https://doi.org/10.1021/am502925j.